

# Onset of Antiferromagnetism in heavy fermion metals.

A. Schröder<sup>1</sup>, G. Aeppli<sup>2</sup>, R. Coldea<sup>3,4</sup>, M. Adams<sup>4</sup>, O. Stockert<sup>1,5</sup>, H.v. Löhneysen<sup>1</sup>, E. Bucher<sup>6,7</sup>, R. Ramazashvili<sup>8</sup> and P. Coleman<sup>9</sup>

<sup>1</sup> *Physikalisches Institut, Universität Karlsruhe, D-76128 Karlsruhe, Germany*

<sup>2</sup> *NEC, 4 Independence Way, Princeton, NJ 08540, U.S.A.*

<sup>3</sup> *Oak Ridge National Laboratory, Oak Ridge, TN 37831, U.S.A.*

<sup>4</sup> *ISIS Facility, CCLRC, Rutherford- Appleton Laboratory, Didcot OX11 0QX, UK*

<sup>5</sup> *present address: University of Bristol, Bristol BS8 1TL, UK*

<sup>6</sup> *Universität Konstanz, D-78457 Konstanz, Germany*

<sup>7</sup> *Bell Laboratories, Lucent Technologies, Murray Hill, NJ 07974, U.S.A.*

<sup>8</sup> *Department of Physics, University of Illinois, Urbana, IL 61801, U.S.A.*

<sup>9</sup> *Materials Theory Group, Rutgers University, Piscataway, NJ 08855, U.S.A.*

There are two views of antiferromagnets. The first proceeds from atomic physics, which predicts that atoms with unpaired electrons develop magnetic moments. In a solid, the coupling between moments on nearby ions then yields antiferromagnetic order at low temperatures<sup>1</sup>. The second, based on the physics of electron fluids or 'Fermi liquids', states that Coulomb interactions can drive the fluid to adopt a more stable configuration by developing a spin density wave.<sup>2,3</sup> It is presently unknown which view is appropriate at a 'quantum critical point', where the antiferromagnetic transition temperature vanishes<sup>4-7</sup>. Here we describe an atomically local contribution to the magnetic correlations which develops in the metal  $\text{CeCu}_{6-x}\text{Au}_x$  at the critical gold concentration ( $x_c = 0.1$ ) where the magnetic ordering temperature is tuned to zero. This contribution implies that a Fermi-liquid destroying spin-localizing transition, unanticipated for the spin density wave description, coincides with the antiferromagnetic quantum critical point

$\text{CeCu}_6$ <sup>8,9</sup> is a "heavy fermion" compound, a class of metal formed between actinide or rare earth elements and transition or noble metals. 'Heavy' refers to the extremely large effective masses of the charge carriers at low temperatures, often hundreds or even thousands of times greater than the electron mass. Because of their large effective electron masses and proximity to antiferromagnetism<sup>10,11</sup>, heavy fermion materials are ideal venues for observing the competition between metallic electron band formation and magnetism. The large masses imply small bandwidths, and the magnetism is easily tuned by external pressure<sup>12</sup>, magnetic field and chemical composition. Thus, all of the phenomena associated with the competition can be readily accessed at low temperatures where it is much easier to collect clean data than for other materials, such as the transition metals or their oxides<sup>13,7</sup>, which also display competition between band formation and magnetism but whose characteristic temperatures are much higher. Because of a substantial data base<sup>14-18</sup> and the ability to grow large and

highly homogeneous single crystals, we have chosen  $\text{CeCu}_{6-x}\text{Au}_x$  as a test material. The quantum critical point (QCP) occurs as gold is substituted for the Cu atoms; when more than 0.1 Cu sites per cerium are replaced<sup>19</sup>, the heavy fermion paramagnet gives way to an ordered antiferromagnet<sup>20,21</sup> (Fig.1a).

Fig.1 illustrates two competing models of magnetic order in rare earth metals that have been widely discussed in the context of heavy fermion systems<sup>22–25</sup>. The fundamental parameter is the strength of the hybridization  $W$  between the localized f orbitals and the more extended s, p and d orbitals. When  $W$  is small, the extended orbitals form a metal which is weakly coupled to the unfilled, and hence magnetic, f-orbitals. Thus, as  $T$  is reduced, the two subsystems undergo largely independent evolutions towards Fermi liquid and magnetically ordered ground states, a situation found in many elemental rare earths (e.g. gadolinium), and their compounds. The volume bounded by the Fermi surface is “small”, containing only electrons from the extended orbitals. As we begin to increase  $W$ , the magnetic coupling between the rare earth ions via the conduction electrons and the magnetic ordering (or “Néel”) temperature,  $T_N$ , both increase. On the other hand, if  $W$  is large, the material develops a Fermi liquid of strongly hybridized carriers with a “large” Fermi volume containing electrons from both extended and f orbitals. The kinetic energy of band electrons then overwhelms interaction effects, with the result that  $T_N$  is suppressed to zero for  $W$  beyond a critical value  $W_c$ <sup>10</sup>.

A key scale for heavy fermion materials is the “Kondo temperature”  $T_K$ : the temperature below which the magnetic susceptibility saturates and the hybridization of the f-orbitals with the other orbitals becomes apparent. In contrast to  $T_N$ , the Kondo temperature  $T_K$ , increases monotonically with  $W$ . The central open question concerns how this scale behaves near the quantum critical point: in particular, whether it remains finite, (Fig. 1b) or whether  $T_K$  and  $T_N$  vanish at the same point (Fig. 1c). The first scenario is required if the local moments are quenched at a finite temperature above the quantum critical point: here, local moments do not play a role in the physics of the quantum critical point and a spin-density wave model must be used.<sup>5,23,24</sup> In the second case, local moments are present at all temperatures down to  $T = 0$  at the QCP, so a heavy electron Fermi surface ceases to exist at the quantum critical point. The present paper gives comprehensive evidence in favor of the second scenario, fig.1(c).

To discriminate between the local-moment and spin-density-wave visions, we have measured the magnetic response function  $\chi(\mathbf{q}, E)$ , as a function of temperature ( $T$ ) and external magnetic fields ( $H$ ), using neutron scattering and bulk magnetometry. The function  $\chi(\mathbf{q}, E)$  describes the Fourier components at frequencies  $E/\hbar$  of the magnetization  $\delta m(\mathbf{q}, t) = \chi(\mathbf{q}, t)\delta h_o$  induced by a unit external field pulse  $\delta h(\mathbf{r}, t) = \delta h_o e^{i\mathbf{q}\cdot\mathbf{r}}\delta(t)$  with spatial modulation described by the wavevector  $\mathbf{q}$ . A particularly simple impulse response is an exponential decay,  $\chi(\mathbf{q}, t) \propto \exp[-\frac{\Gamma_{\mathbf{q}}}{\hbar}t]$ , where  $\Gamma_{\mathbf{q}}/\hbar$  is the magnetic decay rate, for which

$$\chi(\mathbf{q}, E) = A/(\Gamma_{\mathbf{q}} - iE), \quad (1)$$

where  $A$  is a constant. The exponential form is typical for paramagnetic rare-earth insulators where the magnetization is not conserved. To understand how  $\Gamma_{\mathbf{q}}$  can depend on temperature, recall that the zero-energy response is the static magnetic susceptibility, which in paramagnetic insulators follows a Curie-Weiss law  $\chi(\mathbf{q}, E)|_{E=0} = C/(T + \theta(\mathbf{q}))$  with Curie constant  $C$  and  $\mathbf{q}$ -dependent Weiss temperature  $\theta(\mathbf{q})$ . At  $\mathbf{q} = 0$  this is just the uniform sus-

ceptibility, which can be directly measured using a magnetometer. Comparison with eq. (1) leads to the conclusion that  $\Gamma_{\mathbf{q}} = a(T + \theta(\mathbf{q}))$  where  $a = A/C$ . Hence, in paramagnetic insulators, the inverse magnetic response function

$$\chi^{-1}(\mathbf{q}, E, T) = \chi_0^{-1}(E, T) + \theta^\alpha(\mathbf{q})/C \quad (2)$$

is a sum of a non-local, purely  $\mathbf{q}$ -dependent piece  $\theta^\alpha(\mathbf{q})/C$  (here with  $\alpha = 1$ ) and a local ( $\mathbf{q}$ -independent) driving term  $\chi_0^{-1} = (T - iE/a)/C$ . Thus  $T$  and  $iE/a$  are interchangeable in expressions for  $\chi(\mathbf{q}, E)$ , and at critical wavevectors, i.e. the points in the Brillouin zone where  $\theta(\mathbf{q}) = 0$ ,  $\chi = \chi_0$  exhibits  $E/T$  scaling, meaning that

$$\chi_0 = T^{-\alpha} g(E/T) = E^{-\alpha} j(T/E) \quad (3)$$

where  $j(1/y) = y^\alpha g(y)$ . In the simple Curie-Weiss example,  $\alpha = 1$  and  $g(y) = g_0(y) = C/(1 - iy)$  with  $y = E/aT$ .

While  $E/T$ -scaling at critical wavevectors is well-known and established<sup>7,13,26,17</sup>, it does not capture the general dependence of  $\chi$  on wavevector, magnetic field, and zero-temperature tuning parameter (e.g. pressure or composition) for the quantum phase transition. However, inspection of the Curie-Weiss example suggests a set of hitherto untested scaling laws and data replottting procedures. The first follows from insertion of the  $T \rightarrow 0$  limit of eq.(3) into eq. (2). The outcome is that  $\chi^{-1}(\mathbf{q}, E, T = 0)$  displays  $E/\theta(\mathbf{q})$  scaling, i.e.

$$\chi(T \rightarrow 0) = \theta(\mathbf{q})^{-\alpha} G(E/\theta(\mathbf{q})) \quad (4)$$

In the simple Curie-Weiss case  $G(\delta) = g(\delta)$  (with  $\delta = E/a\theta$ ), which is easily understood if we regard excursions in wavenumber or quantum control parameter as excursions in an effective Curie temperature. Letting  $E \rightarrow 0$  instead of  $T \rightarrow 0$  in eq.(3) and again inserting the result into eq.(2) gives a second verifiable relation,

$$\chi^{-1}(\mathbf{q}, T) = (T^\alpha + \theta(\mathbf{q})^\alpha)/C, \quad (5)$$

Eq.(5) implies that the traditional Curie-Weiss plot, where  $1/\chi$  is a straight line as a function of  $T$ , can be replaced across a series of experiments where the Weiss temperature is varied (e.g. by varying  $\mathbf{q}$  or composition  $x$ ) by a plot where  $1/\chi$  as a function of  $T^\alpha$  is a straight line with intercept  $\theta(\mathbf{q})^\alpha$ .

Finally, combining the knowledge that for local moment systems, the magnetic response is governed by the ratio of the Zeeman energy  $g\mu_B H$  to the thermal energy  $k_B T$ , with eq.(2) yields another scaling law, namely

$$(\chi(H, T)^{-1} - \theta(0)^\alpha/C)^{-1} T^\alpha = f(H/T) \quad (6)$$

The law eq.(6) can be tested with extraordinary sensitivity in the long wavelength ( $q = 0$ ) limit using bulk magnetometry.

For systems in which the critical magnetic degrees of freedom derive from spin-density fluctuations of a Fermi sea, matters are much more complicated and do not satisfy eqs(2)-(6). Here we expect that non-local terms, derived from the band-structure, should have both  $E$ - and  $T$ -dependence. At low  $T$ , the first correction to the  $T = 0$  Pauli susceptibility is of order  $T^2$  rather than  $T^\alpha$ , as suggested by the generalized Curie-Weiss Ansatz. Also,  $T$  and

$iE$  are not interchangeable in the temperature-dependent susceptibility. In particular, above two dimensions,<sup>4</sup> the quantum critical fluctuations of a spin density wave are non-interacting at low energies and long wavelengths, in which case  $E/T$  scaling<sup>7</sup> never occurs. Likewise, none of the less familiar forms (4)-(6) accounting for the  $\mathbf{q}$ -,  $T$ -,  $x$ -, and  $H$ -dependence should obtain. Of special significance is that an external magnetic field modifies the band structure, implying an influence on the non-local terms and an inability to scale the field-dependent effects simply in terms of the ratio  $g\mu_B H/k_B T$ .<sup>29</sup>

We have thus reduced the problem of discriminating between the scenarios in figs.1b) and c) to discovering whether the largely untested laws (4)-(6) describe the  $H$ -,  $T$ -,  $E$ -, and  $x$ - dependent magnetic response of  $\text{CeCu}_{6-x}\text{Au}_x$ , and to verifying that with an order of magnitude improvement in energy range,  $E/T$ - scaling obtains at the critical composition and wavevector. To carry out this ambitious program, we have taken advantage of a low-T dc magnetometer<sup>27</sup> and the IRIS spectrometer<sup>28</sup> at the ISIS spallation source. IRIS represents a substantial improvement over the instruments previously used to examine the magnetic fluctuations in  $\text{CeCu}_{5.9}\text{Au}_{0.1}$  in that it (a) surveys the magnetic fluctuation spectrum over a very wide range of wavenumbers, (b) has an energy resolution  $9\mu\text{eV} \equiv 0.1K$  almost an order of magnitude better than that of previous experiments, and (c) yields data in absolute units established using the simultaneously measured elastic incoherent scattering from the sample.

As  $x$  is varied in  $\text{CeCu}_{6-x}\text{Au}_x$ , Bragg reflections due to antiferromagnetism appear at specific wavenumbers on a “butterfly”-shaped critical line<sup>16</sup>, (black crosses in fig 2a). At the quantum critical concentration  $x = x_c$ , the Bragg peaks are replaced by magnetic critical scattering - peaked on the same “butterfly”<sup>15</sup>. Fig. 2b) and c) show scans through the butterfly, obtained for the very small energy  $E = 35\mu\text{eV}$ . On warming from 50 mK to  $0.4K \approx E/k_B$ , the magnetic response at the butterfly is somewhat reduced, while on going to  $1.5K = 4E/k_B$ , it is greatly suppressed, showing that when  $T$  crosses  $E/k_B$ , the magnetic response begins to change rapidly. Fig. 2a shows energy scans collected at 50mK at the various (nearly) fixed momentum transfers indicated in the inset and plotted following the new scaling paradigm eq(4), using the exponent  $\alpha \approx 0.75$  obtained from the  $E/T$  scaling found in our previous critical wavenumber ( $\mathbf{q} = (1.2, 0, 0)$ ) experiment<sup>17</sup> and verified with much greater confidence below. The data collapse onto a single curve is clearly consistent with eq(4), but there is sufficient scatter to mandate checks of the other untested laws (5) before we can claim to have verified the local moment scenario giving rise to eq(2).

Fig.3 shows the modified Curie-Weiss plots suggested by eq(5) for  $\text{CeCu}_{6-x}\text{Au}_x$ , where the effective Weiss temperature is varied either by changing  $q$  in the neutron scattering experiment, or by changing  $x$  in the bulk (low field) magnetometry. Near the quantum critical point, the static susceptibility follows the modified Curie-Weiss law over the entire two-decade temperature range of our measurements. As  $x$  moves away from  $x_c$  in either direction,  $\chi^{-1}(T)$  becomes more curved as  $T \rightarrow 0$ , although there still is a quantum critical regime bounded by a cross-over temperature which increases with distance from  $x_c$  and above which the  $T^\alpha$  power law seems to hold (Fig. 3b), and below which a tendency towards less singular (heavy) Fermi liquid behavior is seen. Fig.3a also demonstrates that at quantum criticality (i.e.  $x \approx 0.1$ ) the same law is followed for general  $\mathbf{q}$ , where  $\chi'(\mathbf{q})$  is obtained via the Kramers-Kronig relation from the neutron data. Indeed, the parallelism of the lines in Fig.3a shows not only that a single exponent  $\alpha$  is sufficient to account for all of the

magnetometry and neutron data, but also that the Curie constant  $C$  is - within the limited statistical accuracy of the latter - the same for all wavenumbers. The overlap between the neutron data at  $\mathbf{q} = (1.8, 0, 0)$  far from the butterfly but close to  $(2, 0, 0)$ , equivalent to  $(0, 0, 0)$ , and the  $\mathbf{q} = 0$  bulk results is reassuring and shows that  $\mathbf{q} = 0$  is a typical non-critical wavenumber, with a spectrum likely to resemble that measured at  $\mathbf{q} = (1.8, 0, 0)$ . A final result which can be extracted from Fig.3 is another estimate of the wavenumber-dependent Weiss temperature  $\theta(\mathbf{q})$ , which is simply the  $x$ -axis intercept, taken to the power  $1/\alpha$ , of the lines going through the data for each  $\mathbf{q}$ . The outcome is entirely consistent with that of the  $E/\theta(\mathbf{q})$  scaling analysis in fig.2a).

We finally turn to the energy- and  $T$ -dependent spectroscopies with the best signal to noise ratios, namely the neutron measurements of the scattering with  $\mathbf{q}$  on the butterfly and the  $H$ - dependent static magnetization. Fig 4a shows the former, plotted versus  $E/T$ , collected at a wavenumber  $(0.8, 0, 0)$ . This data set, which densely covers four decades of  $E/T$ , confirms that the scaling is optimal (see left inset) for  $\alpha = 0.75 \pm 0.05$ . Fig4b shows the collapse of the bulk magnetization data as suggested by the  $H/T$  scaling form (6). The similarities in the scaling function and exponent ( $\alpha = 3/4$ ), obtained in this entirely independent assay, to those obtained via neutron measurements demonstrates that the magnetic response is driven by a singular local term. Two interesting details emerge. First, the effective moment (for definition see Fig 4)  $\mu = g\mu_B = 1.5\mu_B$  is the same order as an atomic moment ( $0.6\mu_B$ ) estimated from considering the  $q$ -space average of the neutron data integrated to  $E = 1\text{meV}$ . This rules out large, randomly occurring ferromagnetic clusters as a key feature of the quantum critical point.<sup>30</sup> Second, the scaling function  $f(h)$  (where  $h = g\mu_B H/k_B T$ ) has the power-law asymptote  $h^{-\alpha}$  at large  $h$ , which decays much more slowly than the  $\exp(-h)$  asymptote derived from the Brillouin function. Thus, the active ingredient responsible for the critical behavior is an atomically local magnetic moment, with a size comparable with a single spin  $S = 1/2$  with an intrinsically critical response to an external field.

Our experiments reveal that the magnetic fluctuations in the heavy fermion metal  $\text{CeCu}_{6-x}\text{Au}_x$  are extraordinarily simple near the quantum critical point at  $x = 0.1$ . Not only do our new high-resolution neutron data satisfy  $E/T$  scaling at the critical wavenumbers with much greater certainty than before, but they together with magnetization data satisfy two hitherto untested scaling laws and a generalized Curie-Weiss paradigm, all of which emerge from a local moment scenario for the quantum critical point. Detailed quantitative analysis (see figure captions) reveals that an algebraic form,

$$\chi^{-1}(\mathbf{q}, E, T) = \left[ \left( T^2 + \left( \frac{g\mu_B}{k_B} \right)^2 H^2 \right)^{1/2} - iE/a \right]^\alpha + \theta(\mathbf{q})^\alpha \Big] C^{-1} = \chi_0^{-1}(E, T) + \theta(\mathbf{q})^\alpha / C \quad (7)$$

accounts for all of our  $H$ -  $\mathbf{q}$ - and  $T$ - dependent results. Eq(7) is the most straightforward generalization of the Curie-Weiss description of a critical point and has only three inputs, an overall amplitude, an exponent  $\alpha$  and the function  $\theta(\mathbf{q})$ .

Clearly then, in answer to the question posed in the introduction, whether an itinerant (fig.1b) or local (fig.1c) picture of the magnetic quantum critical point applies to this heavy fermion system, it is the local scenario (fig.1c) that is appropriate. Beyond this, the most striking feature of the results is the appearance of a single unusual exponent  $\alpha = 0.75$  in the scaling properties at widely different wave-vectors. The  $E/T$  and  $H/T$  scaling with

the unusual exponent  $\alpha = 0.75 < 1$  means that the magnetic properties of  $\text{CeCu}_{6-x}\text{Au}_x$  are more severely non-analytic than those of both Fermi liquids and conventional insulating magnets, where  $\alpha = 1$ .

We conclude that a Fermi liquid,  $\text{CeCu}_6$ , with one of the largest known effective carrier masses is remarkably close to an instability marked by a new kind of critical behavior where the moments associated with the tightly bound f electrons are on the brink of separation from the conduction electrons- how close is apparent from the approach of the inverse magnetic susceptibility to the anomalous  $T^\alpha$  asymptote as  $T$  rises above 2K( fig.3b). The locality of the quantum fluctuations in the ordered phase suggests the development of a new kind of localized excitation, one derived from the ambiguity of whether the f-electrons are counted within the Fermi sea or not. These excitations are neither heavy quasi-particles nor conventional spin excitations and might best be regarded as Fermi surface “shredders”: new degrees of freedom which are ultimately responsible for the non-Fermi liquid behavior and the unusual local scaling behavior at the quantum critical point.

## REFERENCES

- <sup>1</sup> Anderson, P. W. New approach to the theory of superexchange interactions. *Phys. Rev.* **115**, 2 (1959).
- <sup>2</sup> Stoner, E. C. *Phil. Mag* **15**, 1018 (1933); *Proc. R. Soc.* **A154**, 656 (1936).
- <sup>3</sup> Overhauser, A. W. & Arrott, A. Mechanism of antiferromagnetism in chromium. *Phys. Rev. Lett.* **4**, 226 (1960).
- <sup>4</sup> Hertz, J. A. Quantum critical phenomena. *Phys. Rev.* **B 14**, 1165-1184 (1976);
- <sup>5</sup> Millis, A. J. Effect of a nonzero temperature on quantum critical points in itinerant fermion systems. *Phys. Rev. B* **48**, 7183-7196 (1993).
- <sup>6</sup> Chakravarty, S., Halperin, B. I. and Nelson, D. R. Low temperature behavior of a 2D quantum antiferromagnet, *Phys. Rev. Lett.*, 1057 (1988).
- <sup>7</sup> Sachdev, S. & Ye, J. Universal quantum-critical dynamics of two-dimensional antiferromagnets. *Phys. Rev. Lett.* **69**, 2411-2414 (1992).
- <sup>8</sup> Stewart, G. R., Fisk, Z. & Wire, M. S. New Ce heavy-fermion system: CeCu<sub>6</sub>. *Phys. Rev. B* **30**, 482-484 (1984),
- <sup>9</sup> Onuki, Y., Shimizu, Y. & Komatsubara, T. Magnetic property of a new Kondo lattice intermetallic compound: CeCu<sub>6</sub>. *J. Phys. Soc. Jpn* **53**, 1210-1213 (1984)
- <sup>10</sup> Doniach, S. The Kondo lattice and weak antiferromagnetism. *Physica B* **91**, 231-234 (1977);
- <sup>11</sup> Aeppli, G. & Broholm, C. in *Handbook on the Physics and Chemistry of Rare Earths* Magnetic correlations in heavy fermion systems: neutron scattering from single crystals. Vol 19, ed. by Gschneidner, K. A. Jr. *et al.*, (Elsevier, 1994), p. 123-175
- <sup>12</sup> Mathur, N. D. *et al.* Magnetically mediated superconductivity in heavy fermion compounds. *Nature* **394**, 39-43 (1998).
- <sup>13</sup> Varma, C. M., Littlewood, P. B. & Schmitt-Rink, S., Abrahams, E., Ruckenstein, A. E. Phenomenology of the normal state of Cu-O high temperature superconductors. *Phys. Rev. Lett.* **63**, 1996-1999 (1989);
- <sup>14</sup> Löhneysen, H. v. *et al.* Non-Fermi-liquid behavior in a heavy-fermion alloy at a magnetic instability, *Phys. Rev. Lett.* **72**, 3262 (1994).
- <sup>15</sup> Stockert, O., Löhneysen, H. v., Rosch, A., Pyka, N. & Loewenhaupt, M. Two-dimensional fluctuations at the quantum-critical point of CeCu<sub>6-x</sub>Au<sub>x</sub>. *Phys. Rev. Lett.* **80**, 5627-5630 (1998)
- <sup>16</sup> Löhneysen, H. v. *et al.* Magnetic order and transport in the heavy-fermion system CeCu<sub>6-x</sub>Au<sub>x</sub>. *Eur. Phys. J. B* **5**, 447-456 (1998)
- <sup>17</sup> Schröder, A., Aeppli, G., Bucher, E., Ramazashvili, R. Coleman, P. Scaling of magnetic fluctuations near a quantum phase transition. *Phys. Rev. Lett* **80**, 5623-5626 (1998)
- <sup>18</sup> Rosch, A., Schröder, A., Stockert, O. & Löhneysen, H. v. Mechanism for the non-Fermi-liquid behavior in CeCu<sub>6-x</sub>Au<sub>x</sub>. *Phys. Rev. Lett.* **79**, 159-162 (1997)
- <sup>19</sup> Ruck, M. *et al.* Structure and electrical resistivity of the heavy fermion compound CeCu<sub>5</sub>Au. *Act. Cryst.B* **49**, 936-941 (1993)
- <sup>20</sup> Schröder, A., Lynn, J. W., Erwin, R. W., Loewenhaupt, M. & Löhneysen, H. v. Magnetic structure of the heavy fermion alloy CeCu<sub>5.5</sub>Au<sub>0.5</sub>. *Physica B* **199-200**, 47-48 (1994)
- <sup>21</sup> Stockert, O. *et al.* Incommensurate antiferromagnetism and magnetic correlations in CeCu<sub>6-x</sub>Au<sub>x</sub>. *Physica B* **230-232**, 247-249 (1997)

- <sup>22</sup> Si, Q., Smith, J.L & Ingersent, K. Quantum critical behavior in Kondo systems. *Int'l J. Mod. Phys.***13**, 2331-2342 (1999).
- <sup>23</sup> A. Rosch, Interplay of disorder and spin fluctuations in the resistivity near a quantum critical point *Phys. Rev. Lett* **82**, 4280 (1999).
- <sup>24</sup> S. Doniach, Phase Diagram of the Kondo Lattice, in Proceedings of the 5th International Conference on Valence Fluctuations, Plenum, 179-85, (1988)
- <sup>25</sup> Moriya, T. and Takimoto, T. Anomalous properties around magnetic instability in heavy electron systems, *J. Phys Soc. Japan*, **64**, 960 (1995).
- <sup>26</sup> Aronson, M. C. *et al.* Non-Fermi-liquid scaling of the magnetic response in  $\text{UCu}_{5-x}\text{Pd}_x$  ( $x=1,1.5$ ). *Phys. Rev. Lett.* **75**, 725-728 (1995)
- <sup>27</sup> Schröder, A., Schlager, H. G., Löhneysen, H. v. Magnetization of  $\text{CeCu}_6$  at low temperatures, *J. Magn. Magn. Mater.* 108, 47-49 (1992)
- <sup>28</sup> C.J.Carlile & M.A.Adams, The design of the IRIS inelastic neutron spectrometer and improvements to its analysers, *Physica B*, **182** 431-440(1992).
- <sup>29</sup> Sachdev, S. Quantum phase transitions and conserved charges. *Z. Phys. B* **94**, 469-479 (1994)
- <sup>30</sup> Castro Neto, A. H., Castilla G., Jones B. A. Non-Fermi liquid behavior and Griffiths phase in f-electron compounds. *Phys. Rev. Lett.* **81**, pp.3531-4, (1996) USA.



## ACKNOWLEDGMENTS

A. S., O. S. and H. v. L. acknowledge financial support from the Deutsche Forschungsgemeinschaft. R. C. acknowledges financial support from the Oak Ridge National Laboratory Postdoctoral Research Associates Program administered jointly by the Oak Ridge National Laboratory and the Oak Ridge Institute for Science and Education. P. C. and R. R. acknowledge the support of the National Science Foundation.

## Figure Captions

**Fig. 1. Phase diagram and scenarios for quantum criticality in  $CeCu_{6-x}Au_x$**  a) Phase diagram for  $CeCu_{6-x}Au_x$ , where increasing Au-concentration  $x$  drives the heavy fermion alloy into an antiferromagnetically ordered state. The quantum critical point at  $x = 0.1$  is the subject of this paper. b)-c) Two competing models for the magnetic quantum critical point in heavy fermions.  $W$  is the strength of the hybridization between the localized f-electrons and the surrounding conduction sea, which causes the antiferromagnetic order (with transition temperature  $T_N$ ) to collapse at a critical value  $W = W_c$ . (b) The local moments are magnetically quenched - absorbed into the metallic bands- at a finite "Kondo" temperature,  $T_K$  and do not play a role at the quantum critical point. Antiferromagnetism develops via a "spin-density-wave instability" of the underlying Fermi surface. (c) Local moments exist down to an effective lattice Kondo temperature,  $T_K^*$ , which vanishes at the quantum critical point. In this model, local moments become quenched precisely at the quantum critical point, and play an active role in the magnetic critical fluctuations.

**Fig. 2. Magnetic neutron scattering data.** (a) Spectra at wavevectors  $\mathbf{q}$  indicated in inset, as a function of energy transfer  $E$  in units of the  $\mathbf{q}$ -dependent Weiss temperature  $\theta(\mathbf{q})$ . Intensities are correspondingly normalized to  $\theta(\mathbf{q})^{-\alpha}$  ( $\alpha = 0.75$ ), as suggested by eq.(4). The line is the scaling function  $G(\delta) = C/(1 + (-i\delta)^\alpha)$  with  $\delta = E/(aT)$ . The inset is a map of reciprocal space showing the critical line (black lines) close to the magnetic Bragg peaks in the ordered regime (black crosses) and the considered wave vector regions (labeled A-H). **b,c**, Wavevector ( $\mathbf{q}$ ) dependence of the magnetic fluctuations along the middle (**b**) and lower (**c**) trajectory in the inset of (**a**) for fixed  $E = 0.035 meV$ .  $\chi'' = S(1 - e^{-E/k_B T})$  is shown, where the non-magnetic background, derived from scans with  $q$  parallel to the easy moment direction  $c$ , has been subtracted. Different colours represent different temperatures. Lines correspond to Eq.(7) by  $H = 0$  and a temperature independent  $\theta(\mathbf{q})^\alpha$  expanded in even powers of  $\mathbf{q}$ .

**Fig. 3. Temperature dependence of the inverse static susceptibility.** (a)  $\chi(\mathbf{q})$  (from direct magnetization ( $\mathbf{q} = 0$ ) and neutron data ( $\mathbf{q} \neq 0$ )), showing the same anomalous power-law dependence on temperature, over a wide range of different momentum values (see inset in fig.2a). b) Checking the same anomalous power-law in temperature of  $1/\chi(\mathbf{q} = 0)$  for different Au concentrations  $x$ . The temperature below which deviations occur increases with distance to the critical concentration  $x = 0.1$ .

**Fig. 4. Energy and field scaling Plots.**(a)  $E/T$  scaling plots taken at various critical  $\mathbf{q}$  vectors (labelled as A and B as in the inset of fig. (2a)), combining previous triple-axis data with the much more extensive time-of-flight data taken at IRIS. The line is the product of the Bose-Einstein factor  $(1 - e^{-E/k_B T})$  multiplied by the scaling function  $g(y) = C/(1 - iy)^\alpha$  with  $y = E/(aT)$  in eq.(3) with exponent  $\alpha = 0.75$ . Right inset shows the wide range of  $E - T$  covered. Left inset shows the "scatter" of the scaling plot as a function of  $\alpha$ , being minimal for  $\alpha = 0.72 \pm 0.05$ . (b)  $H/T$ -scaling of the local contribution to the uniform magnetization  $M(T, H)$ .  $1/\chi_0 = (dM/dH)^{-1} - (4.1\mu_B^2/meV)^{-1}$ . Solid line corresponds to scaling function  $f(h) = (1 + h^2)^{-\alpha/2}$  with

$h = g\mu_B H/k_B T$  with  $\alpha = 0.75$  and an effective moment  $\mu = g\mu_B = 1.5\mu_B$ . Inset shows the  $H - T$  range where scaling applies.

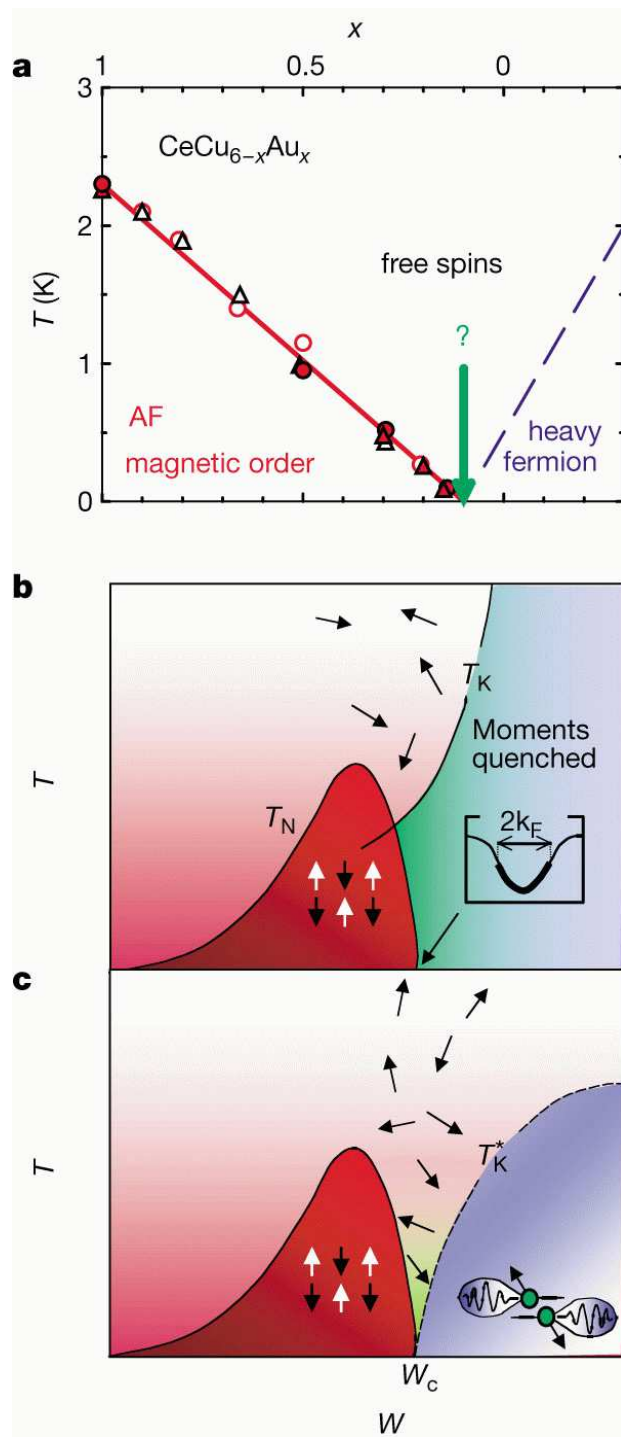


Fig. 1

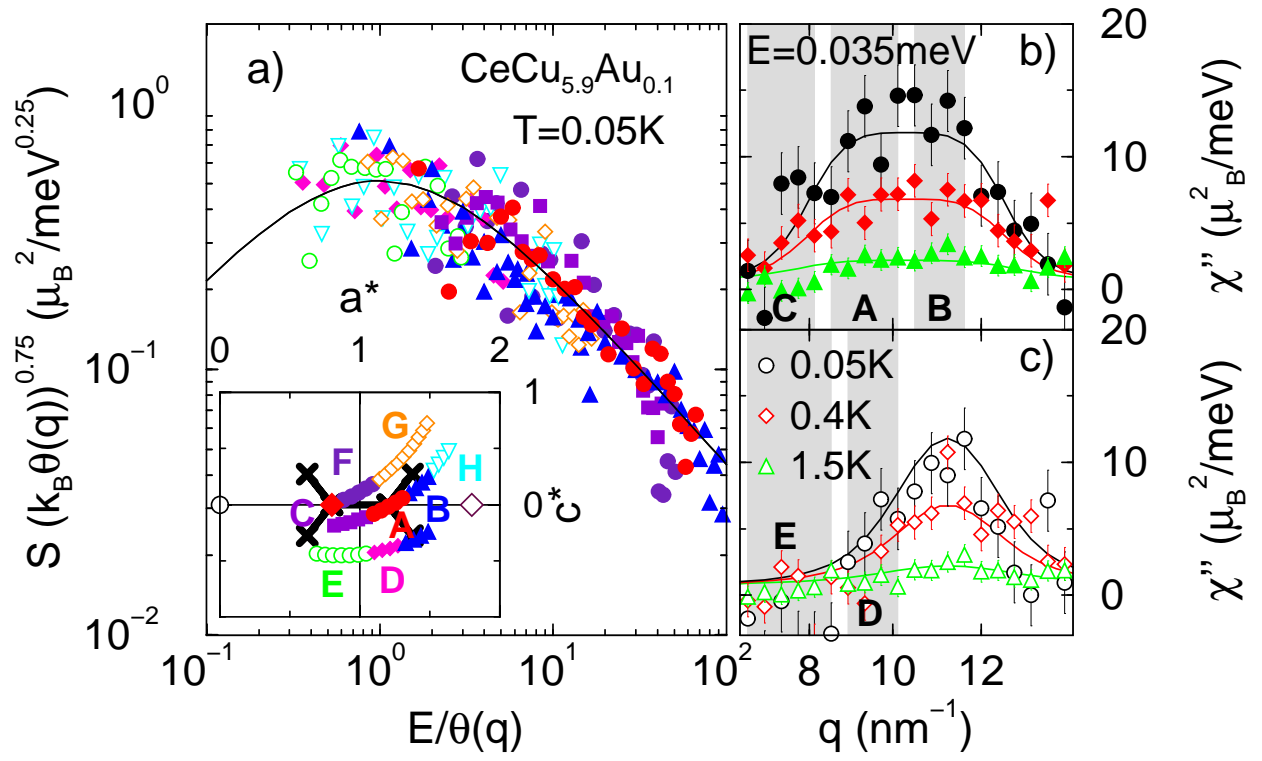


Fig. 2

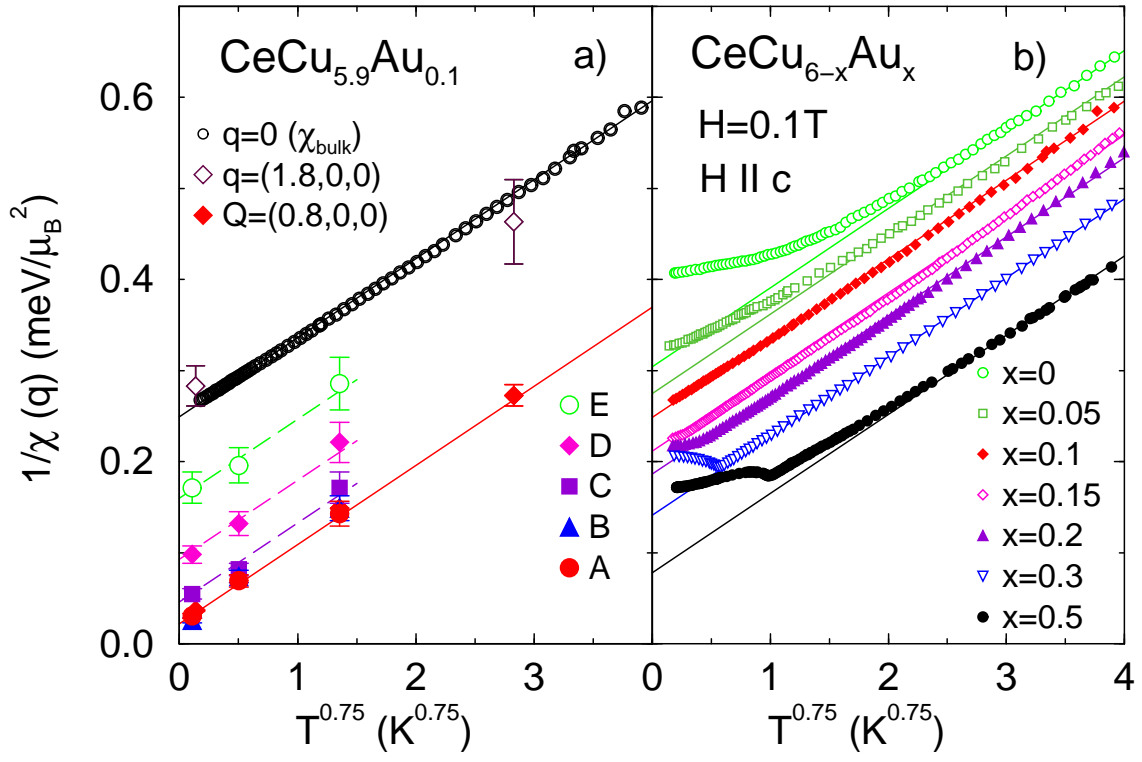


Fig. 3

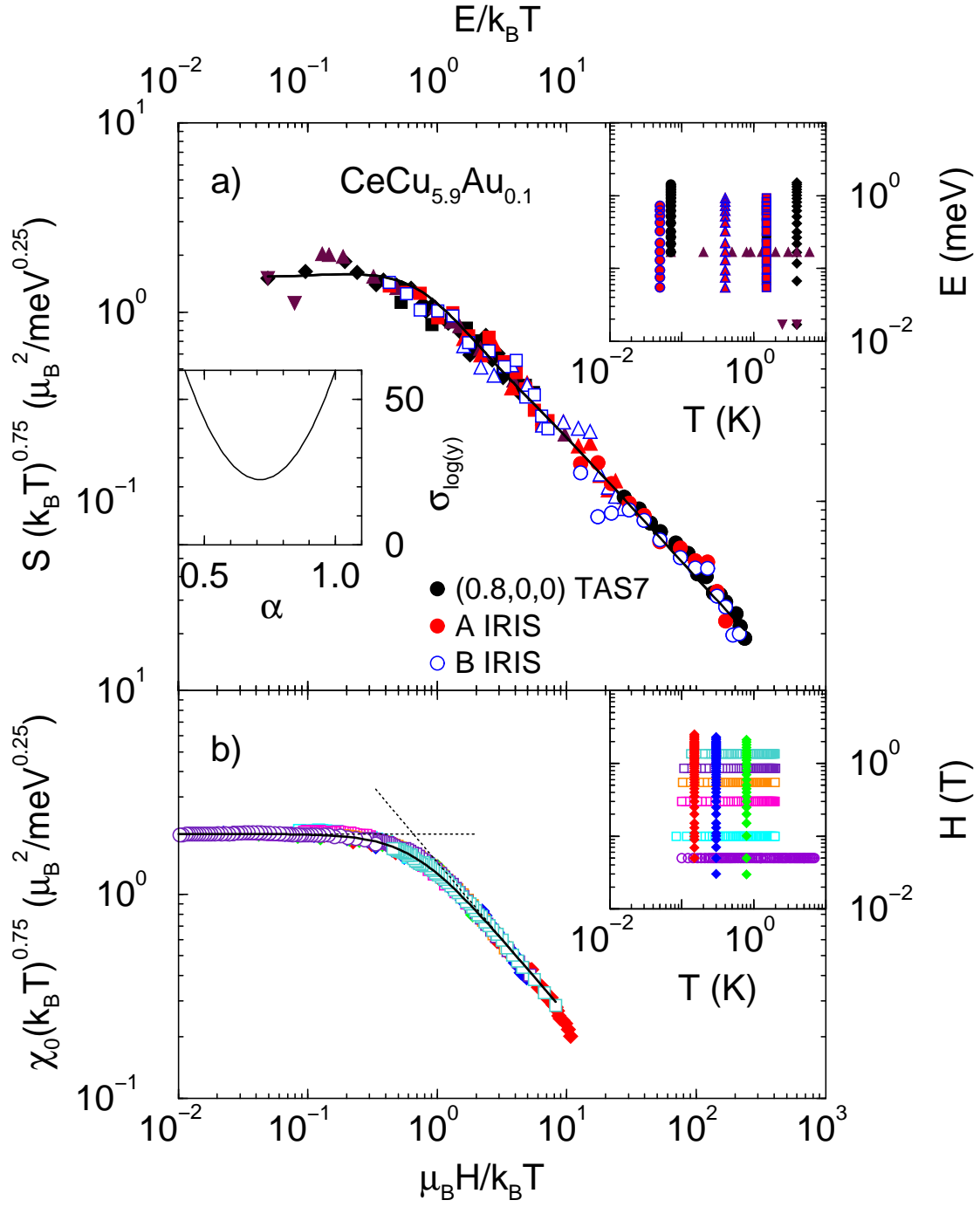


Fig. 4